Smart Structures and Systems, *Vol. 25, No. 5 (2020) 605-617*
DOI: https://doi.org/10.12989/sss.2020.25.5.605

An efficient hybrid TLBO-PSO-ANN for fast damage identification in steel beam structures using IGA

S. Khatir [1a], T. Khatir [2b], D. Boutchicha [3c], C. Le Thanh [1,4d],
H. Tran-Ngoc [1,5e], T.Q. Bui [6,7f], R. Capozucca [8g] and M. Abdel-Wahab [*9,10]

[1] *Soete Laboratory, Faculty of Engineering and Architecture, Ghent University, Technologiepark Zwijnaarde 903, B-9052, Zwijnaarde, Belgium*
[2] *Institute of Science and Technology, Naama University , Algeria*
[3] *University of Science and Technology Oran, Algeria*
[4] *Faculty of Civil Engineering, Open University, Ho Chi Minh City, Vietnam*
[5] *Department of Bridge and Tunnel Engineering, Faculty of Civil Engineering, University of Transport and Communications, Hanoi, Vietnam*
[6] *Institute for Research and Development, Duy Tan University, Da Nang City, Vietnam*
[7] *Tokyo Institute of Technology, Department of Civil and Environmental Engineering, Japan*
[8] *Università Politecnica delle Marche, Ancona, Italy*
[9] *Division of Computational Mechanics, Ton Duc Thang University, Ho Chi Minh City, Vietnam*
[10] *Faculty of Civil Engineering, Ton Duc Thang University, Ho Chi Minh City, Vietnam*

(*Received August 7, 2019, Revised October 25, 2019, Accepted November 25, 2019*)

Abstract. The existence of damages in structures causes changes in the physical properties by reducing the modal parameters. In this paper, we develop a two-stages approach based on normalized Modal Strain Energy Damage Indicator (*nMSEDI*) for quick applications to predict the location of damage. A two-dimensional IsoGeometric Analysis (2D-IGA), Machine Learning Algorithm (MLA) and optimization techniques are combined to create a new tool. In the first stage, we introduce a modified damage identification technique based on frequencies using *nMSEDI* to locate the potential of damaged elements. In the second stage, after eliminating the healthy elements, the damage index values from *nMSEDI* are considered as input in the damage quantification algorithm. The hybrid of Teaching-Learning-Based Optimization (TLBO) with Artificial Neural Network (ANN) and Particle Swarm Optimization (PSO) are used along with nMSEDI. The objective of TLBO is to estimate the parameters of PSO-ANN to find a good training based on actual damage and estimated damage. The IGA model is updated using experimental results based on stiffness and mass matrix using the difference between calculated and measured frequencies as objective function. The feasibility and efficiency of nMSEDI-PSO-ANN after finding the best parameters by TLBO are demonstrated through the comparison with nMSEDI-IGA for different scenarios. The result of the analyses indicates that the proposed approach can be used to determine correctly the severity of damage in beam structures.

Keywords: IsoGeometric Analysis; damage identification; TLBO; PSO-ANN; dynamic analysis

1. Introduction

Many mechanical and civil engineering structures were constructed several decades ago. In order to prevent undesirable failures, many techniques have been developed by researchers in the context of structural health monitoring to predict damage at early stages. The process of damage detection by modal analysis is usually known as vibration-based damage identification, which is classified into four cases: (1) damage existence; (2) localization; (3) quantification; and finally (4) prognosis. Tiachacht *et al*. (2018b) presented a Modified Cornwell indicator for damage quantification. This indicator was investigated numerically using a FEM of truss and 3D structures. (Dahak *et al*. 2017) presented normalized frequencies technique in cantilever steel beam based on experimental results.

The discretization was based on the number of zones in a beam structure. Each zone had a specific classification using the first four natural frequencies. A newly proposed indicator for damage identification based on dynamic analysis in plate-like structures, such as mode shapes and their derivatives, was presented by Navabian *et al*. (2016). Inverse analysis for damage detection in beams using vibration data and a genetic algorithm was presented by Kim *et al*. (2007). Fast crack identification in Carbon Fibre Reinforced Polymer (CFRP) composite structures using model reduction using frequency based on different crack location to build snapshot matrix was presented by Samir *et al*. (2018). This approach was based on measured and

∗Corresponding author, Ph.D., Professor,
E-mail: magd.abdelwahab@tdtu.edu.vn
[a] Ph.D. Student, E-mail: Khatir_samir@hotmail.fr
[b] Professor
[c] Professor
[d] Ph.D. Student
[e] Ph.D. Student
[f] Professor
[g] Professor

http://www.techno-press.org/?journal=sss&subpage=7
ISSN: 1738-1584 (Print), 1738-1991 (Online)

calculated frequencies as objective function using optimization techniques, namely Genetic algorithm (GA) and Cuckoo Search (CS). Furthermore, Khatir *et al*. (2018a) created an application for crack identification in steel beam structures using PSO. The objective function minimizes the measured and calculated frequencies after model updating. Pandey *et al*. (1991) created an approach based on the mode shape curvatures for damage identification. (Wu and Law 2004) presented an application using mode shape curvatures. This application was tested on plate structures. Structural Health Monitoring (SHM) in beam and truss structures using damage indicator, using Frequency Response Function (FRF) was presented by Zenzen *et al*. (2018). The authors extended the work for damage quantification using inverse analysis and calculated and measured FRFs as an objective function using Bat Algorithm. (Capozucca 2014, Capozucca and Bonci 2015) presented a new analytical solution of double notch crack in CRFP beam composite with different boundary conditions. The proposed technique was validated experimentally.

Odessa *et al*. (2019) presented two-step procedure based on the contribution of the analytical platform and the nonlinear response of delaminated sandwich panel. Funari *et al*. (2019) proposed a numerical model using moving mesh technique to predict the crack growth. Inverse analysis for inclusion interfaces identification using XFEM piezoelectric structure was reported by Nanthakumar *et al*. (2016). Vu-Bac *et al*. (2018) used gradient-based optimization algorithms for inverse analysis using measured and calculated displacements at a number of discrete locations. Inverse applications using optimization techniques were presented by Khatir *et al*. (2015, 2018b), Benaissa *et al*. (2017), Samir *et al*. (2018), Tiachacht *et al*. (2018a).

ANN is powerful technique inspired from the biological nervous systems. Recently, this technique was applied to SHM. SHM of beam and bridge using improved ANN technique was presented by Tran-Ngoc *et al*. (2019). The solution of second-order boundary value problems based on ANN methods was presented by Anitescu *et al*. (2019). Delamination detection in composite laminated using MLA was reported by Gomes *et al*. (2019). Abdeljaber *et al*. (2017) provided a convolutional neural network in large-scale steel frame structures for damage detection and localization. Damage identification using FRFs as input data in ANN was studied by Zang and Imregun (2001). Kim *et al*. (2008) used neural networks algorithm for fast damage prediction. Maity and Saha (2004) used back-propagation algorithm in ANN for crack identification using strains and displacements. Guo *et al*. (2019) analyzed bending problem using a deep collocation method (DCM). Damage index data based on Cornwell indicator in laminated composite were collected for PSO-ANN to quantify damage by Khatir *et al*. (2019a).

Hughes *et al*. (2005) created a new powerful numerical tool, namely IGA, which aims to simplify the computer aid design to describe geometry. Thanh *et al*. (2018) used IGA to analyse the static and free vibration of nanoplates using higher order shear deformation theory. Furthermore, using IGA technique, a thermal bending and buckling of composite laminated micro-plate was developed by Thanh *et al*. (2019a) and thermal post-buckling of porous FG micro-plate by Thanh *et al*. (2019b). The authors extended the work to nonlinear static and dynamic responses of FG-CNTRC in Thanh *et al*. (2019c). Thanh *et al*. (2020) used IGA and couple stress theory to analyse complex geometrical structures with internal cutouts. A numerical IGA example of flexoelectric composites was reported by Ghasemi *et al*. (2018) to describe the flexibility of the model as well as to obtain more accurate results. A level-set function based IGA was provided by Ghasemi *et al*. (2017) for topology optimization of flexoelectric materials. Khatir *et al*. (2019b) presented a normalized frequency using MSE combined with two-dimensional IGA model of steel beam. The proposed indicator can predict the damage location with more accuracy. Moreover, the inverse analysis was presented using TLBO and a proposed indicator as an objective function to predict the potential of damage. Khatir and Wahab (2019a, b) presented extended Isogeometric analysis (XIGA) and extended finite element (XFEM) to predict the location and size of crack based on inverse problem using different optimization techniques. The results showed that XIGA has good convergence compared with XFEM.

The main objective of this present study is to enhance the regression of PSO-ANN based on their parameters using TLBO. Beams, which are important structures in civil and mechanical engineering industrial applications, are used as examples and modelled using IGA. Experimental modal analysis using frequency data is performed to validate the proposed application. This paper is organized as follows. In the second section, a brief description of Non-Uniform Rational Basis Spline (NURBS) based IGA analysis is explained. The Hybrid TLBO-PSO-ANN is described in section 3. In section 4, the damage indicator *nMSEDI* is presented. Section 5 presents the numerical damage identification procedures. Experimental validation is presented in section 6 and finally, some concluding remarks are summarized.

2. NURBS based IGA analysis fundamentals

2.1 Basis function

The B-Spline basis function is constructed by the following equation

$$N_{i,p}(\zeta)=\frac{\zeta-\zeta_i}{\zeta_{i+p}-\zeta_i}N_{i,p-1}(\zeta)+\frac{\zeta_{i+p+1}-\zeta}{\zeta_{i+p+1}-\zeta_{i+1}}N_{i+1,p-1}(\zeta)\qquad (p>1) \tag{1}$$

$$N_{i,0}(\zeta)=\begin{cases}1 \text{ if } \zeta_i\le\zeta<\zeta_{i+1}\\ 0 \quad \text{otherwise}\end{cases}\qquad (p=0) \tag{2}$$

In the case of p = 0 and 1, the IGA analysis gives identical results as those of FEM (Hughes, Cottrell, et al. 2005).

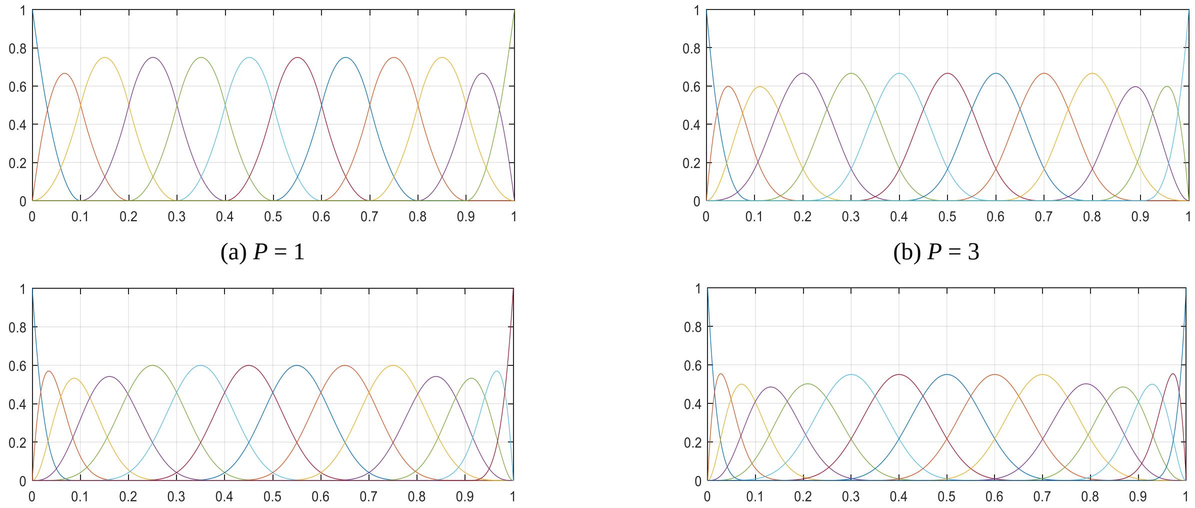

(a) $P = 1$ (b) $P = 3$

(c) $P = 4$ (d) $P = 5$

Fig. 1 B-splines, P = 1, 2, 3, 4 and 5

2.2 The B-spline curve and surface

The B-spline curve $C(\zeta)$ of order p is defined as

$$C(\zeta) = \sum_{i=1}^{n} N_{i,p}(\zeta) P_i \tag{3}$$

where P_i is control points in a bidirectional control net and $N_{i,p}(\xi)$ is B-spline basis function.

A B-spline surface $S(\zeta, \eta)$ is given by

$$S(\zeta,\eta) = \sum_{i=1}^{n}\sum_{j=1}^{m} N_{i,p}(\zeta)\, M_{j,q}(\eta) P_{i,j} \tag{4}$$

Where p and q are the degree of basis function for $N_{i,p}(\zeta)$, and $M_{j,q}(\eta)$ and $P_{i,j}$ are the bidirectional control nets. Eq. (4) can be expressed as follows

$$S(\zeta,\eta) = \sum_{\mathbf{A}}^{n\times m} N_{\mathbf{A}}(\zeta,\eta)\, P_{\mathbf{A}} \tag{5}$$

where $N_{\mathbf{A}}(\zeta,\eta) = N_{i,p}(\zeta) M_{j,q}(\eta)$ is the shape function. NURBS surface $S(\xi,\eta)$ is given by

$$S(\zeta,\eta) = \sum_{\mathbf{A}}^{n\times m} R_{\mathbf{A}}(\zeta,\eta)\, P_{\mathbf{A}}\,; \quad R_{\mathbf{A}} = \frac{N_{\mathbf{A}} w_{\mathbf{A}}}{\sum_{\mathbf{A}}^{n\times m} N_{\mathbf{A}} w_{\mathbf{A}}} \tag{6}$$

Where $w_{\mathbf{A}}$ is the weight function. A quadratic basis functions example is presented in Fig. 1 with different NURBS orders.

3. TLBO-PSO-ANN

3.1 TLBO

TLBO algorithm is introduced by Rao and More (2015). This algorithm is divided into two parts, the first is 'Teacher phase' and the second is 'Learner phase' as explained below.

3.1.1 Teacher phase

This is the first part in which the learners learn from the teacher. For each iteration i, there are 'm' number of subjects used to solve the problem, 'n' number of learners, which present the number of population. If $M_{j,i}$ are the learners results in a particular subject 'j' (j = 1, 2,..., m), then the population ($\mathbf{P_o}$) can be expressed by the following formulation

$$\mathbf{P}_o = \begin{bmatrix} x_{1,1} & x_{1,2} & & & x_{1,n} \\ x_{2,1} & x_{2,2} & & & x_{2,n} \\ \vdots & \vdots & \cdots & \cdots & \vdots \\ \vdots & \vdots & & & \vdots \\ x_{i,1} & x_{i,2} & & & x_{i,n} \end{bmatrix} \tag{7}$$

Where, n is number of the element and i is number of generation.

The best overall result is $X_{total\text{-}kbest,i}$ and all the subjects are presented as the result of best learner k_{best}.

For each subject based on (ΔX) between the corresponding result and existing mean of the teacher is given by the following equation

$$\Delta X = r_i (X_{j,kbest,i} - T_F M_{j,i}) \tag{8}$$

where $X_{j,kbest,i}$ presents the result of the best learner. r_i = [0~1], and T_F is the teaching factor.

The value of T_F can be either 1 or 2 as provided in the following formulation.

$$T_F = round\,[1 + range\,(0{,}1)\{2-1\}] \tag{9}$$

The value of T_F is not a parameter of TLBO, which is determined randomly in Eq. (9).

If T_F = [0~1], the algorithm performs more accurate. The existing solution is updated in the first part according to the following equation

$$X'_{j,k,i} + X_{j,k,i} + \Delta X \tag{10}$$

where, $X'_{j,k,i}$ is the updated value from $X_{j,k,i}$. If $X'_{j,k,i}$ gives better function value, it is accepted.

3.1.2 Learner phase

Secondly, the learners rise their knowledge based on the interaction among themselves. Randomly, two learners P and Q are selected such that

$$X'_{t-P,i} \neq X'_{t-Q,i} \tag{11}$$

where $X'_{t-P,i}$ and $X'_{t-Q,i}$ are the updated function of $X_{t-P,i}$ and $X_{t-Q,i}$ of P and Q, respectively, at the end of the last part presented already, i.e.

$$\begin{aligned} &X''_{j,P,i} = X'_{j,P,i} + r_i\left(X'_{j,P,i} - X'_{j,Q,i}\right), \\ &\text{If} \quad X'_{t-P,i} < X'_{t-Q,i} \end{aligned} \tag{12}$$

$$\begin{aligned} &X''_{j,P,i} = X'_{j,P,i} + r_i\left(X'_{j,Q,i} - X'_{j,P,i}\right), \\ &\text{If} \quad X'_{t-Q,i} < X'_{t-P,i} \end{aligned} \tag{13}$$

The last two equations are used to minimize the problems. Furthermore, to maximise the problems we have to introduce the following formulation.

$$\begin{aligned} &X''_{j,P,i} = X'_{j,P,i} + r_i\left(X'_{j,P,i} - X'_{j,Q,i}\right), \\ &\text{If} \quad X'_{t-Q,i} < X'_{t-P,i} \end{aligned} \tag{14}$$

$$\begin{aligned} &X''_{j,P,i} = X'_{j,P,i} + r_i\left(X'_{j,Q,i} - X'_{j,P,i}\right), \\ &\text{If} \quad X'_{t-P,i} < X'_{t-Q,i} \end{aligned} \tag{15}$$

3.2 Artificial neural network

ANN is a powerful trained technique based on complex input and output datasets from measurements, numerical model or both of them (Rukhaiyar *et al.* 2018). The ANN consists of an input layer, a hidden layer, and an output layer as presented in Fig. 2.

The parameters presented in Fig. 2 are described as follows:

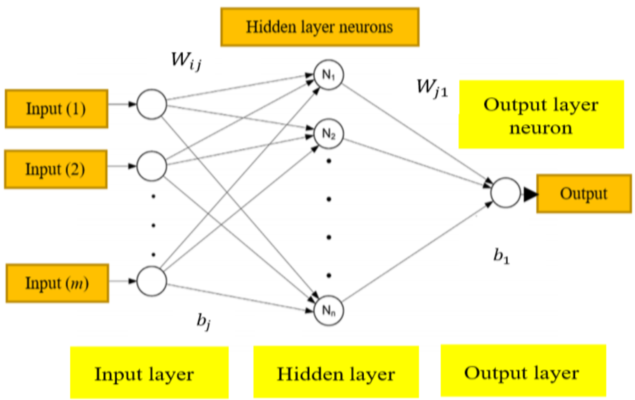

Fig. 2 ANN architecture

(1) W_{ij} is the weight of i^{th} neurons and j^{th} output.
(2) b_j is the bias value of the j^{th} neuron in the hidden layer.
(3) W_j is the weight of neuron, which represents the connection between j^{th} neuron and single neuron in the output.
(4) b_1 is bias associated with the single neuron in output layer neuron.
(5) The indices [i = 1, 2, …, m] are input features from numerical analysis or measurements and [j = 1, 2, …, n] are hidden layer neurons, which can be selected according to the number of data used.

The number of parameters used in the network is $n \times (m + 2) + 1$.

After introducing the data (input and output) for ANN, the training with input and output is performed by PSO based on the best two parameters (weights and biases) of the neurons and it can be used in other optimization techniques. In this paper, we used simple and fast algorithm, namely PSO.

3.3 Objective function

The objective function provided in this paper is to minimize Root-Mean-Square-Error (RMSE), it can be expressed as

$$\text{RMSE} = \sqrt{\frac{\sum_{i=1}^{n}\left(y_{actial} - y_{predicted}\right)^2}{n}} \tag{16}$$

where y_{actual} *and* $y_{predicted}$ are the actual and predicted values and n is number of data.

3.4 PSO

PSO is a bioinspired algorithm proposed by Kennedy (Kennedy 2011). The algorithm uses a set of particles flying in the space to find the global optimum. During an iteration of PSO, each particle update its position according to its previous experience and the experiences of the neighbours. The velocity v_i and the position x_i of each particle will be changed by the best p_{best} and global best value g_{best}. Moreover, two parameters c_1 and c_2 are used for the acceleration.

The objective is to update the positions of each particle in the space as presented in Eqs. (17)-(18). The initial population of size N and dimension D is denoted as $x = [x_1, x_2, \ldots. x_n]^T$.

The individual (particle) x_p (p = 1, 2, …, N) is given as $x_p = [x_{p,1}, x_{p,2}, \ldots. x_{p,D}]$. Moreover, the initial velocity of the population is denoted as $v = [v_1, v_2, \ldots, v_p]^T$ and the velocity of each particle v_p (p = 1, 2, …, N) is given as $v_p = [v_{p,1}, v_{p,2}, \ldots. v_{p,D}]$. The index p varies from [1 to N], whereas the index q varies from [1 to D].

$$\begin{aligned} v_{p,q}^{k+1} = {} & w \times v_{p,q}^{k} + c_1 r_1 \left({p_{best}}_{p,q}^{k} - x_{p,q}^{k}\right) \\ & + c_2 r_2 \left({g_{best}}_{q}^{k} - x_{p,q}^{k}\right) \end{aligned} \tag{17}$$

where r_1 and r_2 are random values generated between [0~1]. Furthermore, the present movement is multiplied by an inertia factor w.

$$x_{p,q}^{k+1} = x_{p,q}^{k} + v_{p,q}^{k+1} \tag{18}$$

Where ${p_{best}}_{p,q}^{k}$ is personal best of the q^{th} component of p^{th} individual. Moreover ${g_{best}}_{q}^{k}$ is q^{th} component of the best individual of the population up to the number of generation k.

3.5 Architecture of TLBO-PSO-ANN

In the first step, the optimum training of ANN using PSO is considered. PSO initialized randomly the two parameters selected, weight and biases, for each iteration based on N sets and size D, respectively. Each set can be presented as the particle of the swarm and as position of the particle.

The fitness for each particle is evaluated, according to the best fitness after each generation and g_{best} and p_{best} are obtained. In the second step, the powerful optimization algorithm TLBO technique is combined with PSO-ANN to find the best parameters of ANN (n number of neurons) and PSO(c_1 and c_2 acceleration factors, population, and generation) for fast and high accuracy prediction of damage. This algorithm is based on the level of damage between real and estimated one, which is used as an objective function. The overall steps of the proposed tool are presented in the flowchart shown in Fig. 3.

4. Normalized Modal Strain Energy Damage Indicator (*nMSEDI*)

For constructing the newly proposed indicator, a modal strain energy formulation is required. Firstly, the free vibration problem is formulated as

$$([K] - {\omega_i}^2[M])\{\phi\}_i = 0, \qquad i = (1,2, \ldots\ldots n) \tag{19}$$

where K is stiffness matrix and M is mass matrix, respectively with $n\times n$ dimensions. ω_i is i^{th} frequency, $\{\phi\}_i$ is mode shapes and n is the number of DOFs according to the number of elements selected.

Secondly, modal strain energies of healthy (MSE_i^u) and damaged (MSE_i^d) structure are presented in the following equations

$$\begin{aligned} MSE^u &= \frac{1}{2}[x_u(\omega)]^T\,[K_e]^u[x_u(\omega)] \\ MSE^d &= \frac{1}{2}[x_d(\omega)]^T\,[K_e]^d[x_d(\omega)] \end{aligned} \tag{20}$$

where, $x(\omega)$ is vector of structural response, ω is frequency, i is mode number and K_e is elementary stiffness matrix.

The total of MSE can be expressed as

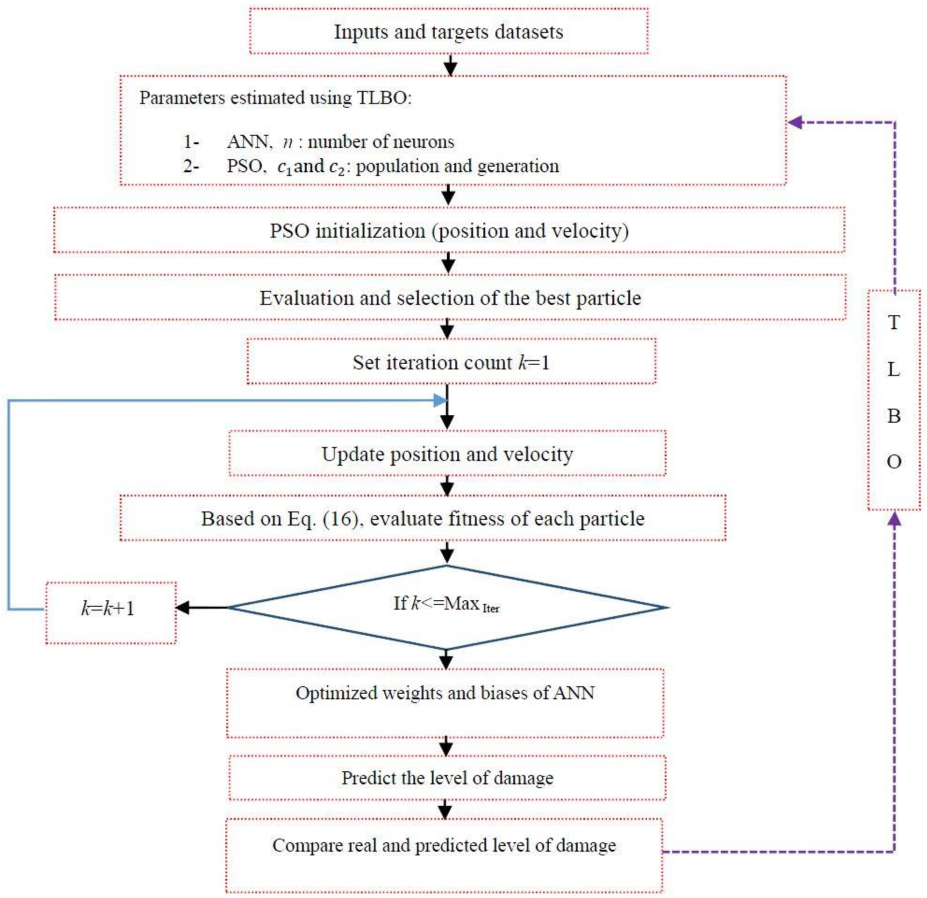

Fig. 3 TLBO-PSO-ANN

Table 1 Mechanical and geometric characteristics of the beam

Properties/unit	value
Young's modulus E (GPa)	210
Width (b) (m)	0.04
Thickness (h) (m)	0.01
Length (L) (m)	1
Mass density (ρ) (kg.m^{-3})	7850
Poison ratio (υ)	0.3

$$MSE_i^{T(u)} = \sum_{e=1}^{n} MSE_i^u \qquad MSE_i^{T(d)} = \sum_{e=1}^{n} MSE_i^d \tag{21}$$

The normalization of $nMSE_i^u$ and $nMSE_i^d$ are presented in the following equation by dividing each elementary energy by the total energy.

$$nMSE_i^u = \frac{MSE_i^u}{MSE_i^{T(u)}}, \qquad nMSE_i^d = \frac{MSE_i^d}{MSE_i^{T(d)}} \tag{22}$$

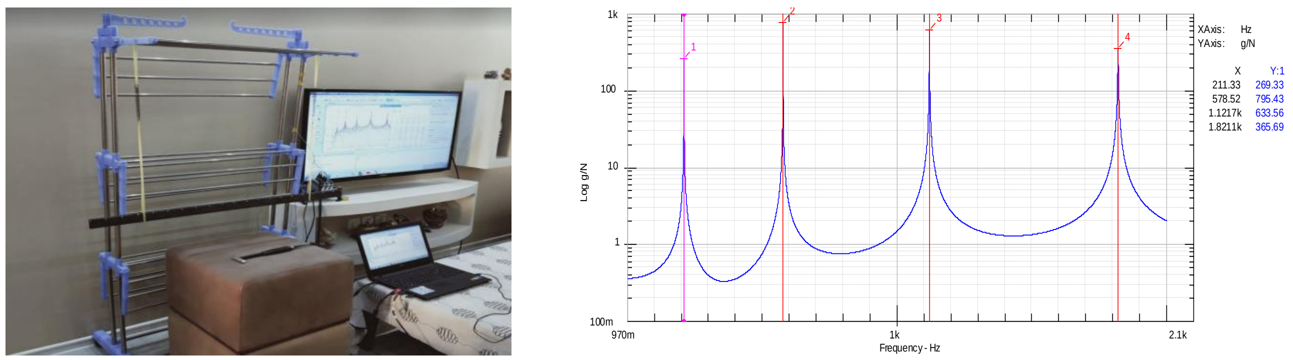

(a) (b)

Fig. 4 Experimental set-up (a) and FRF (b)

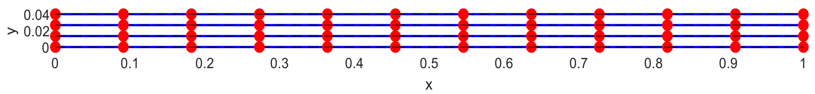

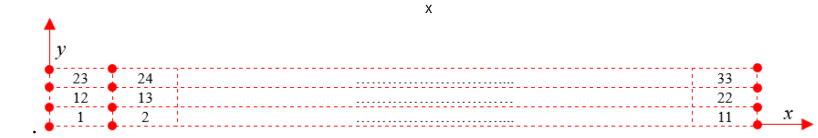

IGA NURBS order 1, 11×3 Elements

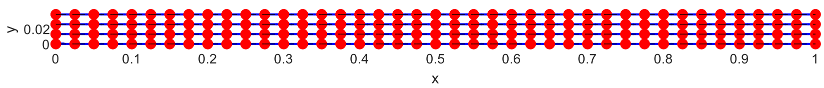

IGA NURBS order 1, 40×3 Elements

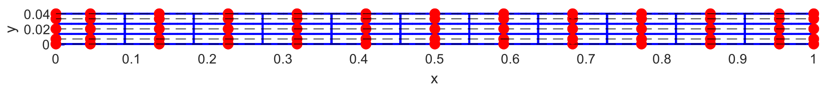

IGA NURBS order 2, 11×3 Elements

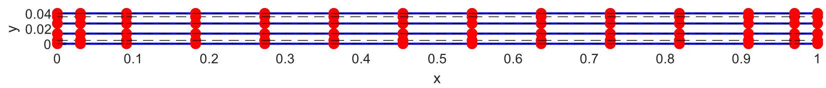

IGA NURBS order 3, 11×3 Elements

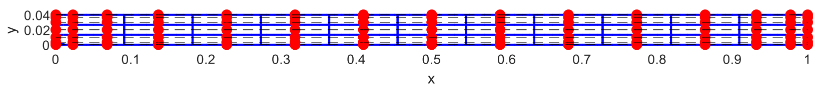

IGA NURBS order 4, 11×3 Elements

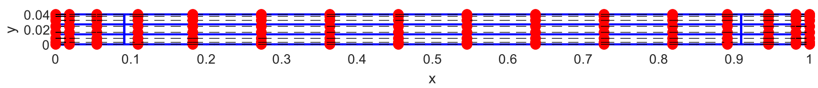

IGA NURBS order 5, 11×3 Elements

Fig. 5 IGA with different NURBS orders

Table 2 Natural frequencies based on IGA and measurements with different NURBS order

Mode	Measurements [Hz]	IGA NURBS order 1 11×3 Elements [Hz]	IGA NURBS order 1 40×3 Elements [Hz]	IGA NURBS order 2 11×3 Elements [Hz]	IGA NURBS order 3 11×3 Elements [Hz]	IGA NURBS order 4 11×3 Elements [Hz]	IGA NURBS order 5 11×3 Elements [Hz]
1	211.33	369.3	223.2	211.9	211.5	211.5	211.5
2	578.52	1031.1	610.4	581.8	576.9	576.9	576.8
3	1121.7	2062.3	1184.0	1139.7	1115.2	1114.3	1114.3
4	1821.1	2595.5	1931.0	1899.2	1813.6	1807.9	1807.6

Table 3 Updated IGA model

Mechanical properties			Frequency			
Parameters	Old	New	Mode	Measurements [Hz]	IGA NURBS order 3 Updated 11×3 Elements [Hz]	Error %
Young modulus (GPa)	210	211.34	1	211.33	211.9	0.269
			2	578.52	578.3	0.038
Density (kg.m^{-3})	7850	7830.81	3	1121.7	1117.9	0.010
			4	1821.1	1818.2	0.159

Table 4 Damage scenarios

Scenario	Damage location	Damage level [%]
1	Element 1	10
2	Element 14	15
3	Element 22	25
4	Element 30	30

In the last step, the first m mode is chosen as effective parameter, and $nMSE^u$ can be expressed by

$$nMSE^u = \frac{\sum_{i=1}^{m} MSE_i^u}{m}, \qquad nMSE^d = \frac{\sum_{i=1}^{m} MSE_i^d}{m} \tag{23}$$

The normalized MSE Damage Indicator (*nMSEDI*) can be expressed by the following formulation

$$nMSEDI = \frac{nMSE^u - nMSE^d}{nMSE^u} \tag{24}$$

The normalized strain energy formulation based on frequency response is used to collect the data with different levels of damage.

5. Results and discussion

In this section, the robustness and effectiveness of the proposed indicator are verified using a free-free beam structure. General information about the characteristics of the beam are presented in Table 1.

For the measurements, we used NI-9234 acquisition card, PCB Accelerometers 356A15, and Hammer PCB 086C03 to analyse the healthy and damaged beams. One accelerometer is used and data are collected at the extremity of beam. The frequencies were calculated after 11 positions of hammer impact.

The experimental set-up, FRF and the first four natural frequencies of healthy beam are shown in Fig. 4.

Fig. 5 presents the different configurations of IGA with different NURBS order. IGA frequencies using different NURBS order and discretization are compared with the measured ones in Table 2. The results showed that IGA with NURBS order 3 is more accurate than other methods.

5.1 Model updating

The model updating is a technique to validate the simulated IGA model of a real structure based on measured frequencies or mode shapes. For this paper, the frequencies used to calibrate the IGA model of the beam structure are obtained by modifying the stiffness and mass matrix based on Young’s modulus and density using TLBO as inverse analysis. The objective function minimizing the differentes between measured and calculated frequencies. The results after model updating are presented in Table 3.

5.2 Damage identification

After model updating, we consider four damage scenarios as presented in Table 4. Based on the damage indicator *nMSEDI*, the results for each scenario are presented in Fig. 6.

It can be seen that *nMSEDI* can predict the correct location of damaged elements. Moreover, it is quite difficult to predict exactly the level of damaged elements for some cases.

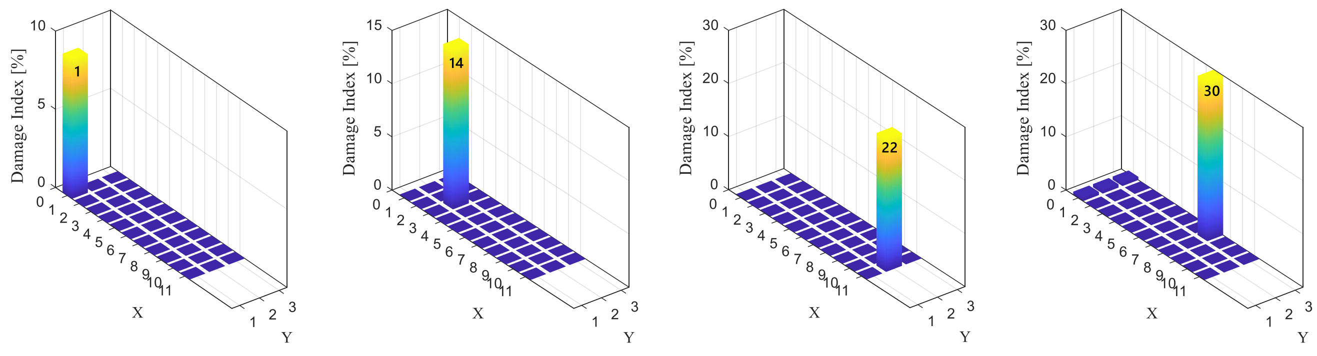

(a) (b) (c) (d)

Fig. 6 Damage index using nMSEDI: (a) scenario 1; (b) scenario 2; (c) scenario 3; and (a) scenario 4

5.3 Application of TLBO-PSO-ANN for damage quantification

In the last stage, we eliminate the healthy elements and predict the level of damage. Vo-Duy *et al*. (2016) used MSE combined with Jaya algorithm to predict the potential of damage in laminated composite plates. Khatir *et al*. (2019b) modified *nMSEDI* and used it as objective function with different optimization techniques to predict the level of damage with high accuracy. However, there are many challenges when using inverse analysis to predict the level of damage. TLBO-PSO-ANN is used as second stage in this paper to predict the level of damage with more accuracy and less CPU time. As presented in the flowchart (see Fig. 3), the TLBO is used to predict the parameters of PSO-ANN and to provide good regression.

5.3.1 Damage scenario 1

In this scenario, local damage is modelled by 30% reduction in stiffness for element 1 to calculate the damage index of *nMSEDI*. The estimated parameters are presented in Table 5. The results using PSO-ANN (before optimizing their parameters) and TLBO-PSO-ANN (using the best parameters) are presented in Fig. 7.

5.3.2 Damage scenario 2

In the second scenario, local damage is modelled by a stiffness reduction of 15% for element 14. The estimated

Table 5 Estimated parameters using TLBO for scenario 1

<table>
<tr><th colspan="2" rowspan="2">TLBO</th><th rowspan="2"></th><th colspan="2">PSO</th><th rowspan="2"></th><th colspan="2">ANN</th></tr>
<tr><th>Without TLBO</th><th>With TLBO</th><th>Without TLBO</th><th>With TLBO</th></tr>
<tr><td rowspan="2">Generation</td><td rowspan="2">100</td><td>Generation</td><td>50</td><td>50</td><td rowspan="3">Number of neurons</td><td rowspan="3">2</td><td rowspan="3">7</td></tr>
<tr><td>Population</td><td>100</td><td>78</td></tr>
<tr><td>Population</td><td>200</td><td>Acceleration factor: $c_1 = c_2$</td><td>0.9</td><td>1.38</td></tr>
</table>

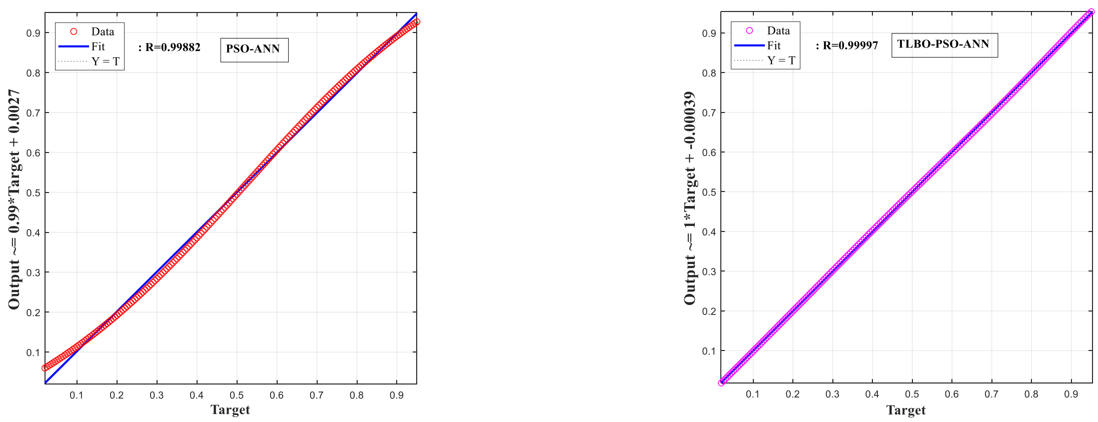

(a) (b)

Fig. 7 (a) Training using PSO-ANN; and (b) Training using TLBO-PSO-ANN (Scenario 1)

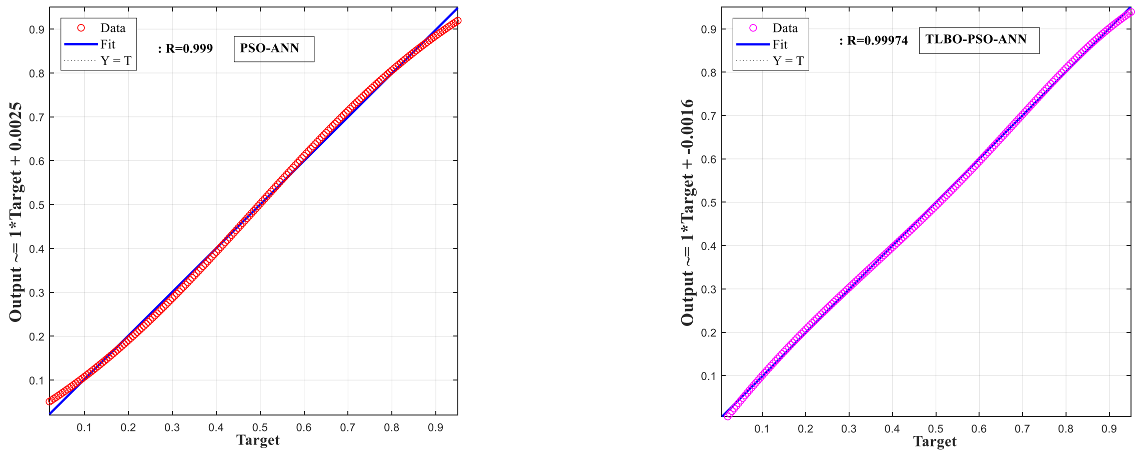

(a) (b)

Fig. 8 (a) Training using PSO-ANN and (b) Training using TLBO-PSO-ANN (Scenario 2)

Table 6 Estimated parameters using TLBO for scenario 2

TLBO			PSO Without TLBO	PSO With TLBO		ANN Without TLBO	ANN With TLBO
Generation	100	Generation	50	42	Number of neurons	2	6
		Population	100	60			
Population	200	Acceleration factor: $c_1 = c_2$	0.9	1.28			

Table 7 Estimated parameters using TLBO for scenario 3

TLBO			PSO Without TLBO	PSO With TLBO		ANN Without TLBO	ANN With TLBO
Generation	100	Generation	50	48	Number of neurons	2	7
		Population	100	90			
Population	200	Acceleration factor: $c_1 = c_2$	0.9	1.45			

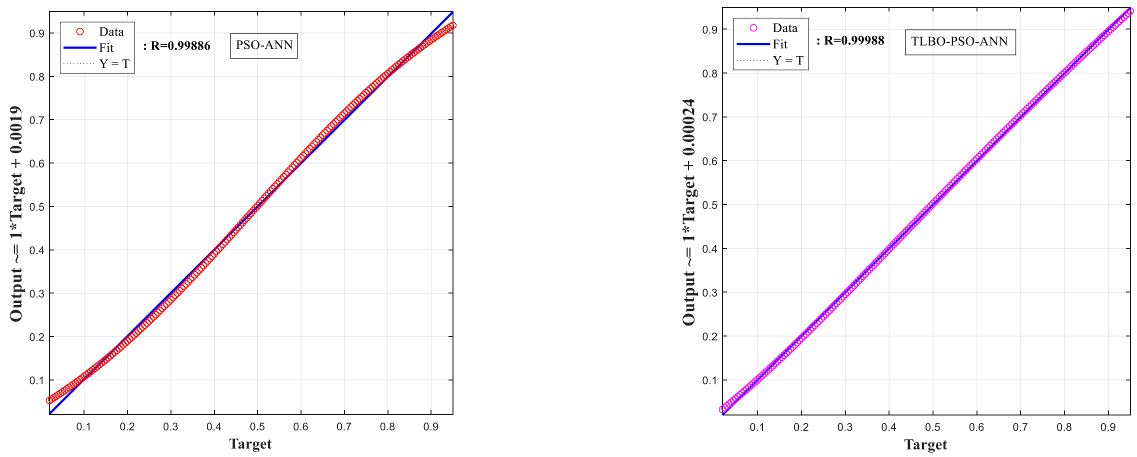

(a) (b)

Fig. 9 (a) Training using PSO-ANN and (b) Training using TLBO-PSO-ANN PSO (Scenario 3)

Table 8 Estimated parameters using TLBO for scenario 4

TLBO			PSO Without TLBO	PSO With TLBO		ANN Without TLBO	ANN With TLBO
Generation	100	Generation	40	56	Number of neurons	2	7
		Population	100	90			
Population	200	Acceleration factor: $c_1 = c_2$	0.8	1.28			

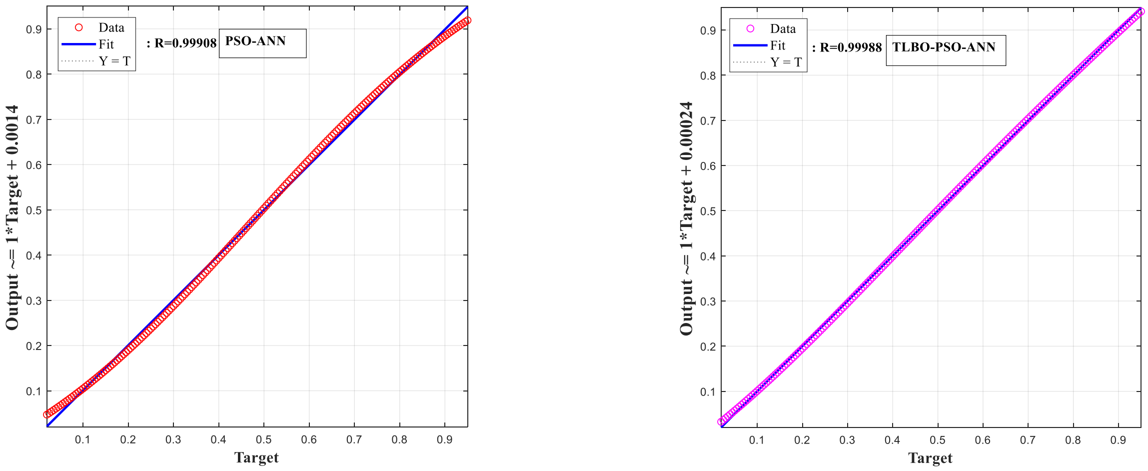

(a) (b)

Fig. 10 (a) Training using PSO-ANN and (b) Training using TLBO-PSO-ANN (Scenario 4)

parameters are provided in Table 6. The results for the second scenario using PSO-ANN and TLBO-PSO-ANN are presented in Fig. 8.

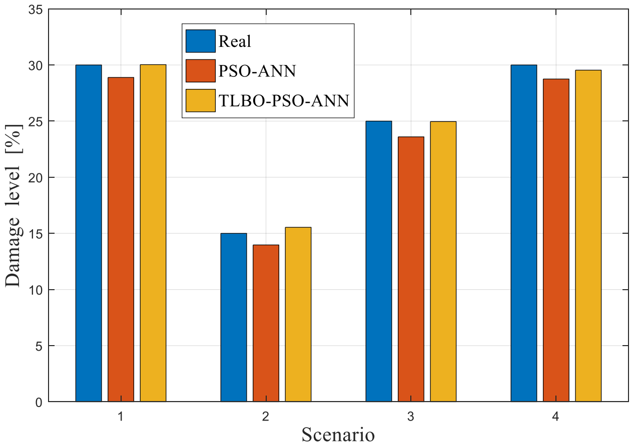

Fig. 11 Comparison between PSO-ANN and TLBO-PSO-ANN for each scenario

5.3.3 Damage scenario 3

In the third scenario, 25% reduction in stiffness in element 22 is introduced to calculate the damage index using *nMSEDI*. The estimated parameters are presented in Table 7. The results using PSO-ANN and TLBO-PSO-ANN are ANN are presented in Fig. 9.

5.3.4 Damage scenario 4

In the last damage scenario, 30% reduction in stiffness in element 30 is introduced. The estimated parameters are presented in Table 8 and the results using PSO-ANN and TLBO-PSO-ANN are presented in Fig. 10.

Fig. 11 summarizes the results of all scenarios before and after damage identification procedures compared with actual damage. The results show that TLBO-PSO-ANN can predict the level of damage more accurate compared with PSO-ANN.

6. Experimental validation

A free-free steel beam is tested experimentally by extending the crack in the middle from 1 till 10 mm as

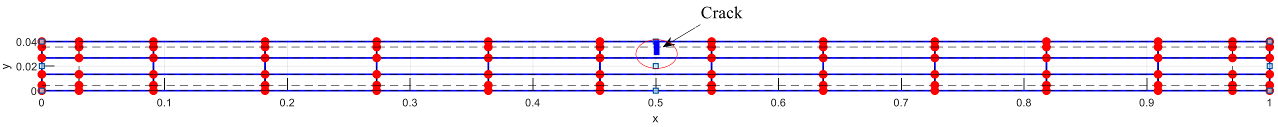

Fig. 12 A free-free steel beam with a crack in the middle

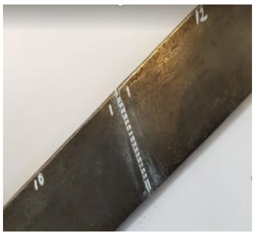

Crack length 2 mm

Crack length 6 mm

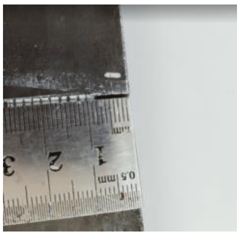

Crack length 8 mm

Fig. 13 Examples of crack configurations

Table 9 Estimated parameters using TLBO based on measured data

Damaged element 28									
Frequency									
Crack 2 mm	Loss of rigidity [%]	Crack 4 mm	Loss of rigidity [%]	Crack 6 mm	Loss of rigidity [%]	Crack 8 mm	Loss of rigidity [%]	Crack 10 mm	Loss of rigidity [%]
210.63		209.53		208.13		205.31		202.81	
577.34	16	577.50	24.63	577.03	34.34	576.72	50.50	577.34	61.95
1118.3		1114.4		1107.8		1095.9		1086.0	
1817.2		1817.7		1816.4		1814.5		1812.9	

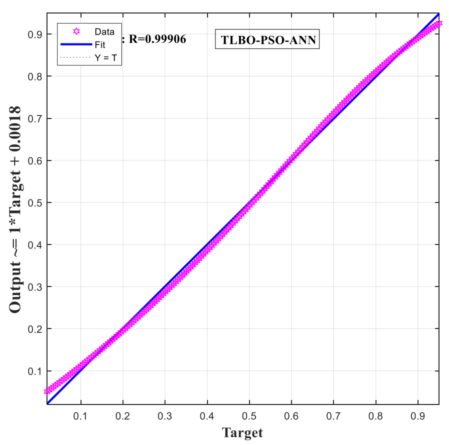

(a)

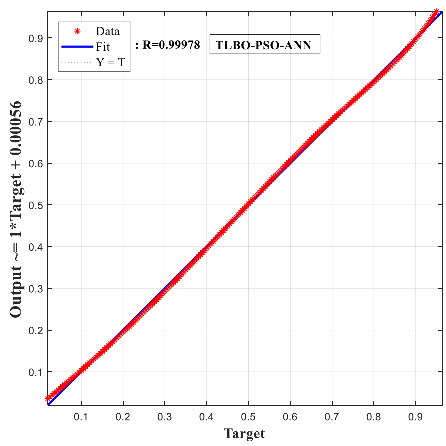

(b)

Fig. 14 Training performance of two damage scenarios: (a) crack length 4 mm and (b) crack length 10 mm

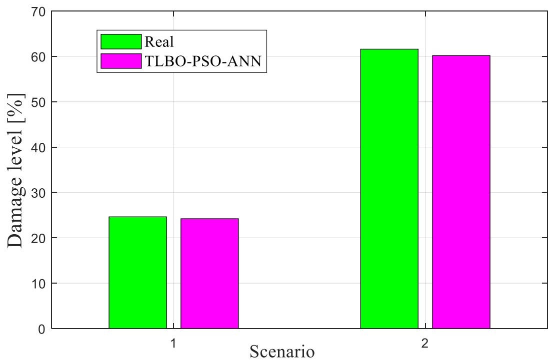

Fig. 15 Level of damage for crack lengths 4 mm and 10 mm calculated by TLBO-PSO-ANN

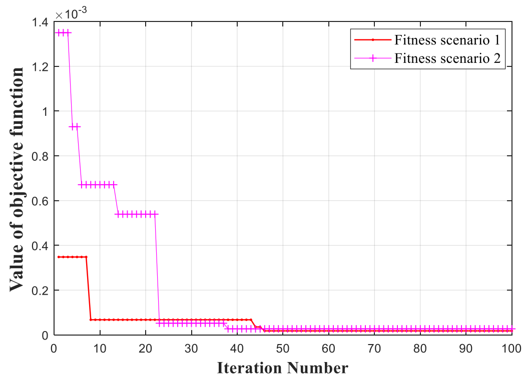

Fig. 16 Fitness of two damage scenarios (crack lengths 4 mm and 10 mm) using TLBO

shown in Fig. 12. Examples of extended crack configuration are presented in Fig. 13.

The crack is simulated by calculating the loss of rigidity in element 28 based on inverse analysis using TLBO after modal updating as presented in Table 9.

From the IGA model, we collect the data based on frequencies and *nMSEDI* values as input and output data. Two scenarios are predicted from Table 9 using TLBO-PSO-ANN. The trained results are presented in Fig. 14. The comparison between real and estimated damages are presented in Fig. 15.

For the training and testing data of *nMSEDI* values and frequencies based on measurements, it can be observed that the best results are obtained when n = 8, swarm size = 86, generation = 67 and acceleration factor $c_1 = c_2$ = 1.19 for the first scenario and the second best when n = 8, swarm size = 75, generation = 70 and acceleration factor $c_1 = c_2$ = 1.15. The fitness of both cases is plotted in Fig. 16.

7. Conclusions

In this present study, a two-stage method using *nMSEDI* and TLBO-PSO-ANN has been proposed for damage detection, localization, and quantification using 2D-IGA model of a beam structure. In the first stage, the damage elements are detected by *nMSEDI* and the healthy elements are eliminated. Whereas, in the second stage, *nMSEDI* is used as input data and TLBO is used to predict the best parameters of PSO-ANN. After collected the new parameters, PSO-ANN is used to estimate the level of damage. Based on the obtained results, some advantages can be presented after using TLBO-PSO-ANN as follows:

(1) The damage indicator, *nMSEDI*, provides good results for damage localization.
(2) *nMSEDI* values are used as input data for training in PSO-ANN.
(3) The proposed application *nMSEDI*-TLBO-PSO-ANN can detect the level of damage correctly with less CPU time after estimating the parameters of PSO-ANN using TLBO.

References

Abdeljaber, O., Avci, O., Kiranyaz, S., Gabbouj, M. and Inman, D.J. (2017), "Real-time vibration-based structural damage detection using one-dimensional convolutional neural networks", *J. Sound Vib.*, **388**, 154-170. https://doi.org/10.1016/j.jsv.2016.10.043

Anitescu, C., Atroshchenko, E., Alajlan, N. and Rabczuk, T. (2019), "Artificial neural network methods for the solution of second order boundary value problems", *Comput. Mater. Continua*, **59**(1), 345-359. https://doi.org/10.32604/cmc.2019.06641

Benaissa, B., Köppen, M., Wahab, M.A. and Khatir, S. (2017), "Application of proper orthogonal decomposition and radial basis functions for crack size estimation using particle swarm optimization", *Journal of Physics: Conference Series, IOP Publishing*, **842**(1), 012014. https://doi.org/10.1088/1742-6596/842/1/012014

Capozucca, R. (2014), "Vibration of CFRP cantilever beam with damage", *Compos. Struct.*, **116**, 211-222. https://doi.org/10.1016/j.compstruct.2014.04.027

Capozucca, R. and Bonci, B. (2015), "Notched CFRP laminates under vibration", *Compos. Struct.*, **122**, 367-375. https://doi.org/10.1016/j.compstruct.2014.11.062

Dahak, M., Touat, N. and Benseddiq, N. (2017), "On the classification of normalized natural frequencies for damage detection in cantilever beam", *J. Sound Vib.*, **402**, 70-84. https://doi.org/10.1016/j.jsv.2017.05.007

Funari, M.F., Lonetti, P. and Spadea, S. (2019), "A crack growth strategy based on moving mesh method and fracture mechanics", *Theor. Appl. Fract. Mech.*, **102**, 103-115. https://doi.org/10.1016/j.tafmec.2019.03.007

Ghasemi, H., Park, H.S. and Rabczuk, T. (2017), "A level-set based IGA formulation for topology optimization of flexoelectric materials", *Comput. Methods Appl. Mech. Eng.*, **313**, 239-258. https://doi.org/10.1016/j.cma.2016.09.029

Ghasemi, H., Park, H.S. and Rabczuk, T. (2018), "A multi-material level set-based topology optimization of flexoelectric composites", *Comput. Methods Appl. Mech. Eng.*, **332**, 47-62. https://doi.org/10.1016/j.cma.2017.12.005

Gomes, G.F., de Almeida, F.A., Junqueira, D.M., da Cunha Jr, S.S. and Ancelotti Jr, A.C. (2019), "Optimized damage identification in CFRP plates by reduced mode shapes and GA-ANN methods", *Eng. Struct.*, **181**, 111-123. https://doi.org/10.1016/j.engstruct.2018.11.081

Guo, H., Zhuang, X. and Rabczuk, T. (2019), "A deep collocation method for the bending analysis of Kirchhoff plate", *CMC-COMPUTERS MATERIALS & CONTINUA*, **59**(2), 433-456. https://doi.org/10.32604/cmc.2019.06660

Hughes, T.J., Cottrell, J.A. and Bazilevs, Y. (2005), "Isogeometric analysis: CAD, finite elements, NURBS, exact geometry and mesh refinement", *Comput. Methods Appl. Mech. Eng.*, **194**(39-41), 4135-4195. https://doi.org/10.1016/j.cma.2004.10.008

Kennedy, J. (2011), "Particle swarm optimization", In: *Encyclopedia of Machine Learning*, Springer, pp. 760-766. https://doi.org/10.1007/978-1-4899-7687-1_630

Khatir, S. and Wahab, M.A. (2019a), "A computational approach for crack identification in plate structures using XFEM, XIGA, PSO and Jaya algorithm", *Theor. Appl. Fract. Mech.*, **103**, 102240. https://doi.org/10.1016/j.tafmec.2019.102240

Khatir, S. and Wahab, M.A. (2019b), "Fast simulations for solving fracture mechanics inverse problems using POD-RBF XIGA and Jaya algorithm", *Eng. Fract. Mech.*, **205**, 285-300. https://doi.org/10.1016/j.engfracmech.2018.09.032

Khatir, S., Belaidi, I., Serra, R., Wahab, M.A. and Khatir, T. (2015), "Damage detection and localization in composite beam structures based on vibration analysis", *Mechanics*, **21**(6), 472-479. https://doi.org/10.5755/j01.mech.21.6.12526

Khatir, S., Dekemele, K., Loccufier, M., Khatir, T. and Wahab, M.A. (2018a), "Crack identification method in beam-like structures using changes in experimentally measured frequencies and Particle Swarm Optimization", *Comptes Rendus Mécanique*, **346**(2), 110-120. https://doi.org/10.1016/j.crme.2017.11.008

Khatir, S., Wahab, M.A., Benaissa, B. and Köppen, M. (2018b), "Crack identification using eXtended IsoGeometric analysis and particle swarm optimization", In: *Fracture, Fatigue and Wear*, Springer, pp. 210-222. https://doi.org/10.1007/978-981-13-0411-8_21

Khatir, S., Tiachacht, S., Thanh, C.L., Bui, T.Q. and Wahab, M.A. (2019a), "Damage assessment in composite laminates using ANN-PSO-IGA and Cornwell indicator", *Compos. Struct.*, 111509. https://doi.org/10.1016/j.compstruct.2019.111509

Khatir, S., Wahab, M.A., Boutchicha, D. and Khatir, T. (2019b), "Structural health monitoring using modal strain energy damage indicator coupled with teaching-learning-based optimization algorithm and isogoemetric analysis", *J. Sound Vib.*, **448**, 230-246. https://doi.org/10.1016/j.jsv.2019.02.017

Kim, J.T., Park, J.H., Yoon, H.S. and Yi, J.H. (2007), "Vibration-based damage detection in beams using genetic algorithm", *Smart Struct. Syst., Int. J.*, **3**(3), 263-280. https://doi.org/10.12989/sss.2007.3.3.263

Kim, J.T., Park, J.H., Koo, K.Y. and Lee, J.J. (2008), "Acceleration-based neural networks algorithm for damage detection in structures", *Smart Struct. Syst., Int. J.*, **4**(5), 583-603. https://doi.org/10.12989/sss.2008.4.5.583

Maity, D. and Saha, A. (2004), "Damage assessment in structure from changes in static parameter using neural networks", *Sadhana*, **29**(3), 315-327. https://doi.org/10.1007/bf02703781

Nanthakumar, S.S., Lahmer, T., Zhuang, X., Zi, G. and Rabczuk, T. (2016), "Detection of material interfaces using a regularized level set method in piezoelectric structures", *Inverse Probl. Sci. Eng.*, **24**(1), 153-176. https://doi.org/10.1080/17415977.2015.1017485

Navabian, N., Bozorgnasab, M., Taghipour, R. and Yazdanpanah, O. (2016), "Damage identification in plate-like structure using mode shape derivatives", *Arch. Appl. Mech.*, **86**(5), 819-830. https://doi.org/10.1007/s00419-015-1064-x

Odessa, I., Rabinovitch, O. and Frostig, Y. (2019), "High-order crack propagation in compressed sandwich panels", *J. Sandw. Struct. Mater.*, 1099636218824873. https://doi.org/10.1177/1099636218824873

Pandey, A.K., Biswas, M. and Samman, M.M. (1991), "Damage detection from changes in curvature mode shapes", *J. Sound Vib.*, **145**(2), 321-332. https://doi.org/10.1016/0022-460x(91)90595-b

Rao, R.V. and More, K.C. (2015), "Optimal design of the heat pipe using TLBO (teaching–learning-based optimization) algorithm", *Energy*, **80**, 535-544. https://doi.org/10.1016/j.energy.2014.12.008

Rukhaiyar, S., Alam, M.N. and Samadhiya, N.K. (2018), "A PSO-ANN hybrid model for predicting factor of safety of slope", *Int. J. Geotech. Eng.*, **12**(6), 556-566. https://doi.org/10.1080/19386362.2017.1305652

Samir, K., Brahim, B., Capozucca, R. and Wahab, M.A. (2018), "Damage detection in CFRP composite beams based on vibration analysis using proper orthogonal decomposition method with radial basis functions and cuckoo search algorithm", *Compos. Struct.*, **187**, 344-353. https://doi.org/10.1016/j.compstruct.2017.12.058

Thanh, C.L., Phung-Van, P., Thai, C.H., Nguyen-Xuan, H. and Wahab, M.A. (2018), "Isogeometric analysis of functionally graded carbon nanotube reinforced composite nanoplates using modified couple stress theory", *Compos. Struct.*, **184**(Supplement C), 633-649. https://doi.org/10.1016/j.compstruct.2017.10.025

Thanh, C.L., Tran, L.V., Bui, T.Q., Nguyen, H.X. and Abdel-Wahab, M. (2019a), "Isogeometric analysis for size-dependent nonlinear thermal stability of porous FG microplates", *Compos. Struct.* https://doi.org/10.1016/j.compstruct.2019.04.010

Thanh, C.L., Tran, L.V., Vu-Huu, T. and Abdel-Wahab, M. (2019b), "The size-dependent thermal bending and buckling analyses of composite laminate microplate based on new modified couple stress theory and isogeometric analysis", *Comput. Methods Appl. Mech. Eng.* https://doi.org/10.1016/j.cma.2019.02.028

Thanh, C.L., Tran, L.V., Vu-Huu, T., Nguyen-Xuan, H. and Abdel-Wahab, M. (2019c), "Size-dependent nonlinear analysis and damping responses of FG-CNTRC micro-plates", *Comput. Methods Appl. Mech. Eng.* https://doi.org/10.1016/j.cma.2019.05.002

Thanh, C.L., Khatir, S. and Wahab, M.A. (2020), "Free Vibration of Angle-Ply Laminated Micro-plates Using Isogeometric Analysis and Modified Couple Stress Theory", *Proceedings of the 13th International Conference on Damage Assessment of Structures*, Springer. https://doi.org/10.1007/978-981-13-8331-1_67

Tiachacht, S., Bouazzouni, A., Khatir, S., Behtani, A., Zhou, Y.L.M. and Wahab, M.A. (2018a), "Structural health monitoring of 3D frame structures using finite element modal analysis and genetic algorithm", *J. Vibroeng.*, **20**(2), 1272-1272. https://doi.org/10.21595/jve.2018.19767

Tiachacht, S., Bouazzouni, A., Khatir, S., Wahab, M.A., Behtani, A. and Capozucca, R. (2018b), "Damage assessment in structures using combination of a modified Cornwell indicator and genetic algorithm", *Eng. Struct.*, **177**, 421-430. https://doi.org/10.1016/j.engstruct.2018.09.070

Tran-Ngoc, H., Khatir, S., De Roeck, G., Bui-Tien, T. and Wahab, M.A. (2019), "An efficient artificial neural network for damage detection in bridges and beam-like structures by improving training parameters using cuckoo search algorithm", *Eng. Struct.*, **199**, 109637. https://doi.org/10.1016/j.engstruct.2019.109637

Vo-Duy, T., Ho-Huu, V., Dang-Trung, H. and Nguyen-Thoi, T. (2016), "A two-step approach for damage detection in laminated composite structures using modal strain energy method and an improved differential evolution algorithm", *Compos. Struct.*, **147**, 42-53. https://doi.org/10.1016/j.compstruct.2016.03.027

Vu-Bac, N., Duong, T.X., Lahmer, T., Zhuang, X., Sauer, R.A., Park, H.S. and Rabczuk, T. (2018), "A NURBS-based inverse analysis for reconstruction of nonlinear deformations of thin shell structures", *Comput. Methods Appl. Mech. Eng.*, **331**, 427-455. https://doi.org/10.1016/j.cma.2017.09.034

Wu, D. and Law, S.S. (2004), "Damage localization in plate structures from uniform load surface curvature", *J. Sound Vib.*, **276**(1-2), 227-244. https://doi.org/10.1016/j.jsv.2003.07.040

Zang, C. and Imregun, M. (2001), "Combined neural network and reduced FRF techniques for slight damage detection using measured response data", *Arch. Appl. Mech.*, **71**(8), 525-536. https://doi.org/10.1007/s004190100154

Zenzen, R., Belaidi, I., Khatir, S. and Wahab, M.A. (2018), "A damage identification technique for beam-like and truss structures based on FRF and Bat Algorithm", *Comptes Rendus Mécanique*, **346**(12), 1253-1266. https://doi.org/10.1016/j.crme.2018.09.003

CC